COMPARATIVE STUDY OF CONTOUR FITTING METHODS IN SPECKLED IMAGES

María E. Buemi, Juliana Gambini, Julio C. Jacobo, Marta E. Mejail
Universidad de Buenos Aires, Facultad de Ciencias Exactas y Naturales, Departamento de Computación
Ciudad Universitaria, Pabellón I, C1428EGA
Ciudad Autónoma de Buenos Aires – República Argentina

Alejandro C. Frery
Universidade Federal de Alagoas, Departamento de Tecnologia da Informação
BR 104 Norte km 97, 57072-970 Maceió, AL – Brazil

Keywords: Speckle, contour fitting, B-Spline, anisotropic diffusion, maximum likelihood.

Abstract: Images obtained with the use of coherent illumination are affected by a noise called speckle, which is inherent to this type of imaging systems. In this work, speckled data have been statistically treated with a multiplicative model using the family of $\mathcal{G}$ distributions. One of the parameters of these distributions can be used to characterize the different degrees of roughness found in speckled data. We used this information to find boundaries between different regions within the image.

Two different region contour detection methods for speckled imagery, are presented and compared. The first one maximizes a likelihood function over the speckled data and the second one uses anisotropic difussion over roughness estimates. To represent detected contours, the B-Spline curve representation is used.

In order to compare the behaviour of the two methods we performed a Monte Carlo experience. It consisted of the generation of a set of test images with a randomly shaped region, which is considered in the literature as a difficult contour to fit. Then, the mean square error was calculated for each test image, for both methods.

1 INTRODUCTION

Several types of imaging devices employ coherent illumination as, for instance, Synthetic Aperture Radar (SAR), sonar, laser and ultrasound-B. The images generated by these devices are affected by a noise called speckle, a kind of degradation that does not obey the classical hypotheses of being Gaussian and additive. Speckle noise reduces the ability to extract information from the data, so specialized techniques are required to deal with such imagery.

Speckled data have been statistically modeled under the multiplicative model using the family of $\mathcal{G}$ distributions, since these probability laws are able to describe the observed data better than other laws, specially in the case of rough and extremely rough areas.

As a case of interest, in SAR images such situations are common when scanning urban spots or forests on undulated relief, and for them the more classical Γ and $\mathcal{K}$ distributions do no exhibit good performance (Frery et al., 1997; Mejail et al., 2001). Under the $\mathcal{G}$ model, regions with different degrees of roughness can be characterized by the parameters. Therefore, this information can be used to find boundaries between regions with different textures.

An example is shown in Figure 1, where the dashed lines show the ideal boundary and the solid lines presents typical speckled data set associated to this edge in semilogarithmic scale. As can be seen in this figure, edge detection in speckled imagery is a tough task due to the low signal-to-noise ratio.

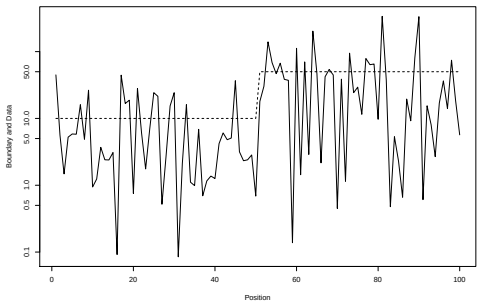

Figure 1: Edge (dashed lines) and speckled data (solid lines).

E. Buemi M., Gambini J., C. Jacobo J., E. Mejail M. and C. Frery A. (2007).
COMPARATIVE STUDY OF CONTOUR FITTING METHODS IN SPECKLED IMAGES.
In *Proceedings of the Second International Conference on Computer Vision Theory and Applications - IFP/IA*, pages 309-316

On the other hand, contours formulated by means of B-Splines present several advantages: allow local control, have local representation, require few parameters and are intrinsically smooth.

We compare two strategies for boundary detection with B-Spline deformable contours: one that maximizes a likelihood function that directly employs the speckled image values that obey a $\mathcal{G}_A^0$ law (Gambini et al., 2006) and another strategy that uses anisotropic diffusion over roughness estimates based on this statistical distribution (Gambini et al., 2004).

In order to compare the behavior of both methods we performed a Monte Carlo experience. It consists of the generation of a set of test images with a randomly shaped region. For 2D shapes of fixed perimeter, (Hero et al., 1999) established that disk-shaped objects are the easiest to estimate, while flower-shaped objects are the hardest to estimate, among the class of objects representable by the B-Spline basis. Then, we generate random samples obeying the $\mathcal{G}_A^0$ distribution with different parameters for the points inside and outside the flower contour. Finally, we calculate the error fitting. We conclude that the maximum likelihood model assuming the $\mathcal{G}_A^0$ distribution for the speckled data is the best of these two edge detection procedures with respect to both the error and the computational cost.

The structure of this paper is as follows: section 2 describes the statistical model used for single channel speckled data, section 3 provides a brief account of B-spline curve fitting, section 4 describes the algorithms in detail, section 5 presents the error evaluation methodology, section 6 presents the results and section 7 concludes the paper.

2 THE $\mathcal{G}$ DISTRIBUTION FOR SPECKLED DATA

Speckled images can be modeled as the product of two independent random fields, one corresponding to the backscatter X and other corresponding to the speckle noise Y (Goodman, 1976):

$$Z = X \cdot Y. \tag{1}$$

For amplitude data, the speckle noise Y is modeled as a $\Gamma^{-1/2}(n,n)$ distributed random variable, where n is the number of looks used to generate the image; this parameter is known or estimated beforehand, and it is valid for the whole image.

The most general model for the backscatter X here considered is the Generalized Inverse Gaussian law (Barndorff-Nielsen and Blaesild, 1983; Jorgensen, 1982; Seshadri, 1993), denoted as $\mathcal{N}^{-1/2}(\alpha,\lambda,\gamma)$. For particular values of the parameters of the $\mathcal{N}^{-1/2}$ distribution, the $\Gamma^{1/2}(\alpha,\lambda)$, and the $\Gamma^{-1/2}(\alpha,\gamma)$ distributions are obtained. These, in turn, give rise to the $\mathcal{K}_A$ and the $\mathcal{G}_A^0$ distributions for the return Z, respectively. See(Mejail et al., 2001).

The $\mathcal{G}^0$ distribution represents an attractive choice for SAR data modeling, given its tractability, expressiveness and capability of retrieving detailed information from the data (Quartulli and Datcu, 2004). Its density function for amplitude data, is given by

$$f_{\mathcal{G}_A^0}(z) = \frac{2n^n(n-\alpha)}{\gamma^\alpha\Gamma(-\alpha)\Gamma(n)}\frac{z^{2n-1}}{(\gamma+z^2n)^{n-\alpha}}, \quad -\alpha,\gamma,z>0,\ n\geq 1. \tag{2}$$

This situation is denoted $Z \sim \mathcal{G}_A^0(\alpha,\gamma,n)$, being its moments

$$E_{\mathcal{G}_A^0}(Z^r) = \left(\frac{\gamma}{2n}\right)^{r/2}\frac{\Gamma(-\alpha+r/2)}{\Gamma(-\alpha)}\frac{\Gamma(n+r/2)}{\Gamma(n)}, \tag{3}$$

if $-\alpha > r$ or infinite otherwise.

Speckled data is described in this paper by the $\mathcal{G}_A^0$ law. Given the data, the statistical parameters are estimated and this information is used to extract region boundaries present in the image.

2.1 Parameter Estimation

As presented in equation (2), the parameter α of the $\mathcal{G}_A^0$ distribution is defined for negative values. Estimation is crucial in many applications and, besides that, the value of this parameter is immediately interpretable in terms of target roughness; this interpretability will be treated in detail in section 2.2.

In this work sample moments parameter estimation method (MO for short) is used. This technique is based on replacing theoretical moments by sample observations, and then calculating the unknown parameters.

To estimate α and γ it is necessary to estimate two moments. In this work moments of order $1/2$ and 1, namely $m_{1/2}$ and m_1 respectively, will be used. From equation (3), these moments are given by

$$m_{1/2} = \left(\frac{\gamma}{n}\right)^{1/4}\frac{\Gamma(-\alpha-1/4)\Gamma(n+1/4)}{\Gamma(-\alpha)\Gamma(n)}, \tag{4}$$

$$m_1 = \left(\frac{\gamma}{n}\right)^{1/2}\frac{\Gamma(-\alpha-1/2)\Gamma(n+1/2)}{\Gamma(-\alpha)\Gamma(n)}, \tag{5}$$

for $\alpha < -1/4$ and $\alpha < -1/2$, respectively. Then, using equations (4) and (5), $\widehat{\alpha}$ can be determined as the solution of

$$g(\widehat{\alpha}) - \zeta = 0, \tag{6}$$

where

$$g(\widehat{\alpha}) = \frac{\Gamma^2\left(-\widehat{\alpha}-\frac{1}{4}\right)}{\Gamma(-\widehat{\alpha})\Gamma\left(-\widehat{\alpha}-\frac{1}{2}\right)} \tag{7}$$

and

$$\zeta = \frac{\widehat{m}_{1/2}^2}{\widehat{m}_1} \frac{\Gamma(n)\Gamma(n+\frac{1}{2})}{\Gamma^2(n+\frac{1}{4})}, \tag{8}$$

and then substituting the value of $\widehat{\alpha}$ in equation (4) or in equation (5) the value of $\widehat{\gamma}$ is found. It can be noticed that $g(\widehat{\alpha})$ converges asymptotically to one as $\widehat{\alpha} \to -\infty$. As ζ is a random variable that can take values greater than one, there are cases for which equation (6) does not have a solution. The lower the value of the α parameter, the higher the probability that a solution for equation (6) does not exist. This issue was solved by (Mejail et al., 2003) replacing unobserved estimates by the median of surrounding values.

2.2 Parameter Interpretation

One of the most important features of the $\mathcal{G}_A^0$ distribution is that the estimated values of the parameter α have immediate interpretation in terms of roughness. For values of α near zero, the imaged area presents very heterogeneous gray values, as is the case of urban areas in SAR images. As we move to less heterogeneous areas like forests, the value of α diminishes, reaching its lowest values for homogeneous areas like pastures and certain types of crops. This is the reason why this parameter is regarded to as a roughness or texture measure.

3 B-SPLINE REPRESENTATION

We use the B-Spline curve representation for describing object contours in a scene. In the following, a brief review of B-Spline representation of contours is presented; for more details see (Blake and Isard, 1998) and (Rogers and Adams, 1990).

Let $\{Q_0, \ldots, Q_{N_B-1}\}$ be a set of control points, where $Q_n = (x_n, y_n)^t \in \mathbb{R}^2$, $0 \le n \le N_B - 1$, and let $\{s_0 < s_1 < s_2 < \cdots < s_{L-1}\} \subset \mathbb{R}$ be a set of L knots. A B-Spline curve of order d is defined as a weighted sum of N_B polynomial basis functions $\mathrm{B}_{n,d}(s)$ of degree $d-1$, within each interval $[s_i, s_{i+1}]$ with $0 \le i \le L-1$. The spline function is $r(s) = (x(s), y(s))^t$, $0 \le s \le L-1$, being

$$r(s) = \sum_{n=0}^{N_B-1} \mathrm{B}_{n,d}(s) Q_n, \tag{9}$$

and

$$x(s) = \mathrm{B}^t(s) Q^x \tag{10}$$

$$y(s) = \mathrm{B}^t(s) Q^y \tag{11}$$

where the basis functions vector $\mathrm{B}(s)$ of N_B components is given by $\mathrm{B}(s) = (\mathrm{B}_{0,d}(s), \ldots, \mathrm{B}_{N_B-1,d}(s))^t$. The weight vectors Q^x and Q^y give the first and second components of Q_n, respectively.

The curves used in this work are closed, with $d = 3$ or $d = 4$, and are specified by periodic B-Spline basis functions.

4 BOUNDARY DETECTION

In this section we present the methods developed to detect region boundaries in speckled imagery.

Let E be a scene made up by a background B and a set of k distinct regions $\{R_1, R_2, \ldots, R_k\}$ with boundaries $\{\partial R_1, \ldots, \partial R_k\}$, respectively. Each of these regions and the background are considered to be random fields of independent, identically distributed, random variables obeying the $\mathcal{G}_A^0$ distribution and characterized by the values of their statistical parameters (α_h, γ_h), $1 \le h \le k$. The only assumption we make is that regions and background have different textures, i.e., if α_0 is the background roughness then $\alpha_h \neq \alpha_0$ for every $1 \le h \le k$.

For each region R_h, we want to find the curve C_h that fits the boundary ∂R_h in the image. As shown in section 2.2, there is a correspondence between the various areas present in the image and the parameters of roughness and scale. From this correspondence a classification of the image can be done.

The algorithms we propose aim at separating regions of a certain specified type from the rest of the image, so we obtain a first rough approximation, or seed: the starting regions of interest. The contour extraction algorithms work over these regions instead of analyzing the whole image reducing, thus, the computational effort.

This initial region detection is computed over non-overlapping blocks of the image using as input the number of blocks and the type of region to be detected (homogeneous, heterogeneous or extremely heterogeneous); the details are presented in (Gambini et al., 2006). Once k regions are identified, each centroid c_h, $1 \le h \le k$, is computed.

If a point belongs to the object boundary, then a sample taken from its neighborhood should exhibit a change in its properties and, therefore, could be considered a transition point. In order to find transition points, N segments $s^{(i)}$, $1 \le i \le N$, of the form $s^{(i)} = \overline{c\,p_i}$ are considered for each region, being c the centroid of the initial region, the extreme p_i a point outside of the region. It is necessary for the centroid c to be in the interior of the object whose contour is sought. A strip $S_h^{(i)}$ is defined over each segment $s^{(i)}$. This procedure is illustrated in the fluxogram of Figure 2 and in Figures 3 and 4 with a SAR image.

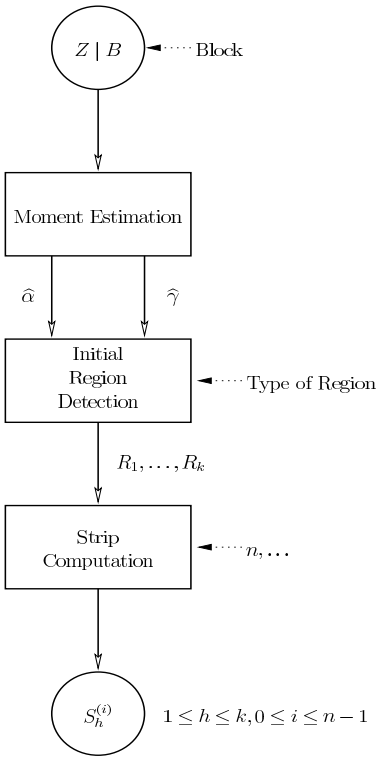

Figure 2: Sequence of operations leading from the data conditioned on the blocks $(Z \mid B)$ to the n strips $S_h^{(i)}$, $0 \le i \le n-1$, for each region $1 \le h \le k \le i \le n-1$, for each region $1 \le h \le k$.

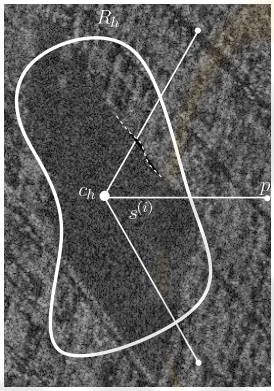

Figure 3: Initial region R_h with the segments $s^{(i)}$, extreme point p_i and center c_h on a SAR image.

In this work we present a comparative study of two new methods for contour detection in speckled imagery using statistical properties of the data and B-Spline curve representation. One of them uses Maximum Likelihood over speckled data and the other uses Anisotropic Diffusion over the roughness estimates.

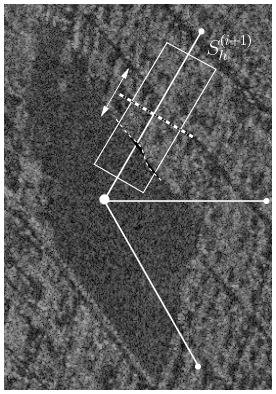

Figure 4: Strip $S_h^{(i+1)}$ defined over the $s^{(i+1)}$ on a SAR image.

As we explain in the following section.

4.1 Maximum Likelihood (ML)

The general problem consists of finding a transition point within each strip $S_h^{(i)}$. These points will be sought using the data along the discrete version of $s^{(i)}$, for which we will not introduce a new notation (see Figure 2):

$$s^{(i)} = \left(z_1^{(i)}, \ldots, z_m^{(i)}\right), \quad 1 \le i \le N. \tag{12}$$

For each segment $s^{(i)}$, $1 \le i \le N$, we consider the following partition

$$Z_k^{(i)} \sim \mathcal{G}_A^0(\alpha_r, \gamma_r), \quad k = 1, \ldots, j \tag{13}$$

$$Z_k^{(i)} \sim \mathcal{G}_A^0(\alpha_b, \gamma_b), \quad k = j+1, \ldots, m \tag{14}$$

where for each k, with $1 \le k \le m$, $z_k^{(i)}$ is the realization of the random variable $Z_k^{(i)}$. The parameters (α_r, γ_r) and (α_b, γ_b) characterize the region and its background, respectively.

In order to find the transition point on each segment $s^{(i)}$, an objective function is considered: the likelihood of the sample which is given by

$$L(j) = \prod_{i=1}^{j} \Pr(z_i; \alpha_r, \gamma_r) \cdot \prod_{i=j+1}^{m} \Pr(z_i; \alpha_b, \gamma_b). \tag{15}$$

Alternatively, we can maximize

$$\begin{aligned} \ell(j) &= \ln L(j) = \sum_{i=1}^{j} \ln(f_{\mathcal{G}^0}(z_i; \alpha_r, \gamma_r)) \\ &\quad + \sum_{i=j+1}^{m} \ln(f_{\mathcal{G}^0}(z_i; \alpha_b, \gamma_b)). \end{aligned} \tag{16}$$

According to equation (2)

$$\ell(j) = \sum_{i=1}^{j} \ln\left(\frac{2n^n\Gamma(n-\alpha_r)z_i^{2n-1}}{\gamma_r^{\alpha_r}\Gamma(-\alpha_r)\Gamma(n)\left(\gamma_r+nz_i^2\right)^{n-\alpha_r}}\right) + \\ + \sum_{i=j+1}^{m} \ln\left(\frac{2n^n\Gamma(n-\alpha_b)z_i^{2n-1}}{\gamma_b^{\alpha_b}\Gamma(-\alpha_b)\Gamma(n)\left(\gamma_b+nz_i^2\right)^{n-\alpha_b}}\right). \quad (17)$$

Finally, the estimated index on the segment that corresponds to the transition point $\widehat{j}$ is given by

$$\widehat{j} = \arg\max_j \ell(j). \quad (18)$$

The scheme of this procedure is shown in Algorithm 1.

Algorithm 1 Edge detection by maximum likelihood using raw data.

1: **for** each segment $s^{(i)}$, $i = 1,\ldots,N$ **do**
2: Estimate the parameters (α_r,γ_r) and (α_b,γ_b).
3: Find the index $\widehat{j}$ on the segment $s^{(i)}$ that maximizes equation (18); it corresponds to the border point b_i in the image.
4: **end for**
5: Build the B-Spline curve that interpolates the boundary points $\{b_1,\ldots,b_N\}$.

In Figure 5 the result of applying algorithm 1 to a real SAR image, is shown.

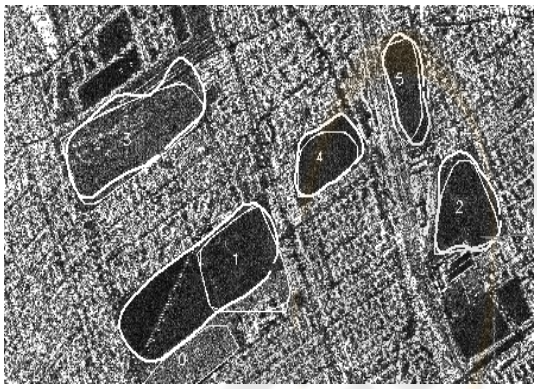

Figure 5: Maximum likelihood edge detection in a SAR image of Munich.

4.2 Anisotropic Diffusion (AD)

Another way of finding the transition point on a line $s^{(i)}$ is to estimate the α parameter in a window centered on each pixel on the line using the data on the strip $S^{(i)}$. Then an array $\widehat{\Lambda}^{(i)} = [\widehat{\alpha}_1^{(i)},\ldots,\widehat{\alpha}_m^{(i)}]$ of estimates of the α parameter is obtained. If a point lies on the boundary between two regions, then it exhibits an abrupt change in the values of the α estimates.

(Perona and Malik, 1990) proposed an algorithm that combats noise preserving boundary features. In its continuous version, it consists of producing a sequence of images $I(\cdot,\cdot,t)$, $t \geq 0$, according to the following equation:

$$\frac{\partial I(x,y,t)}{\partial t} = \nabla \cdot [g(\|\nabla I\|)\nabla I], \quad (19)$$

where $I(\cdot,\cdot,0)\colon \mathbb{R}^2 \to \mathbb{R}^+$ is the original image, t is an artificial time parameter, ∇I is the image gradient, $\|\nabla I\|$ is the image gradient magnitude, '$\nabla\cdot$' denotes the divergence, $g\colon \mathbb{R} \to [0,1]$ is an edge detection function with the only constraints that (i) $g(x) \to 0$ monotonically when $x \to \infty$, and (ii) $g(x) \to 1$ when $x \to 0$. More details can be found in, among others, (Weickert, 1998).

The position of the discontinuity on $s^{(i)}$ is found by convolving the smoothed roughness estimates with a cyclic border detection operator, followed by a convenient thresholding. The scheme of this procedure is shown in Algorithm 2.

Algorithm 2 Edge detection by anisotropic diffusion.

1: **for** each segment $s^{(i)}$, $i = 1,\ldots,N$ **do**
2: Estimate the parameter α for each pixel on $s^{(i)}$ using a sliding window. This generates an array $\widehat{\Lambda}^{(i)} = [\widehat{\alpha}_1^{(i)},\ldots,\widehat{\alpha}_m^{(i)}]$ of estimated values of α.
3: Smooth the array $\widehat{\Lambda}^{(i)}$ using anisotropic diffusion. This generates the smoothed estimates array $\widehat{\Lambda}_S^{(i)}$.
4: Find b_i, the position on line $s^{(i)}$ that corresponds to the maximum discontinuity among the values in the smoothed array $\widehat{\Lambda}_S^{(i)}$ convolving with the mask $[-2,-1,0,1,2]$.
5: **end for**
6: Build the B-Spline curve that interpolates the boundary points $\{b_1,\ldots,b_N\}$.

In Figure 6, the results of applying Algorithm 2, are shown. Having proposed two edge detection techniques, we now proceed to their comparative assessment.

5 CONTOUR FITTING ERROR

This section is devoted to the study of the error committed in the determination of contours by applying the segmentation methods described above to a series of randomly generated images.

Figure 6: Edge detection by anisotropic detection in a SAR image of Munich.

The error evaluation algorithm is applied to a family of synthetic random images of flower shaped regions $\{F_k\}_{k=1,\ldots,n}$. Then, the error of approximating these regions by the obtained B-Spline curves is estimated. The $\{F_k\}_{k=1,\ldots,n}$ are formed in two stages: first a random region is generated, and then the background and foreground are simulated.

The random region boundary is generated according to a parametric curve in polar coordinates given by

$$\begin{aligned} f(s;\eta,\beta,\delta) &= (\theta(s),\rho(s;\eta,\beta,\delta)),\ s\in[0,S] \\ \theta(s) &= s\frac{2\pi}{S} \\ \rho(s;\eta,\beta,\delta) &= \eta-\delta\cos(\beta\theta(s)), \end{aligned} \tag{20}$$

where η is the flower radius, β is the number of petals and 2δ is the petal depth.
In this work the parameters η, β and δ are considered to be independent random variables uniformly distributed the sets $[5,20]$, $\{15,\ldots,50\}$ and $[2,10]$, respectively.

After a region boundary is generated, $\mathcal{G}_A^0$ distributed speckle noise is added to the image. Figure 7shows some of these simulated images, along with the estimated boundaries.

In order to calculate the error in boundary fitting we consider ∂R to be the boundary of the region to be segmented and $\mathcal{C}$ the resulting curve. Let $s^1,\ldots,s^m$ be a set of radial lines given by $s^j=\lambda\vec{u}^j+c\ j=1\ldots m$, where $\vec{u}^j$ is a unitary vector that determines the line direction, and c is the centroid of region R. The point c and the vectors $\vec{u}^j\ j=1,\ldots,m$ are the same for all of the test images. Let $\vec{V}_j$ be the intersection points between curve $\mathcal{C}$ and line s^j, and let $\vec{W}_j$ be the intersection points between curve ∂R and the line s^j:

$$s^j\cap\mathcal{C}=\vec{V}_j,\quad s^j\cap\partial R=\vec{W}_j. \tag{21}$$

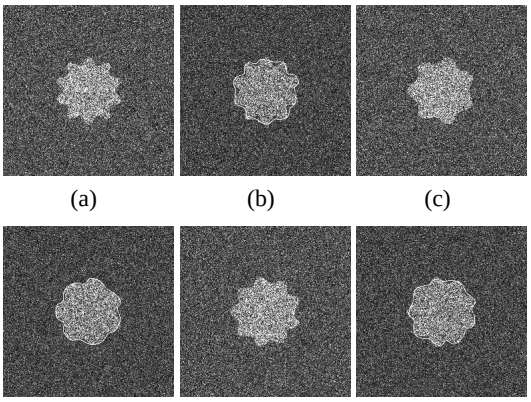

Figure 7: Synthetic images and detected boundaries with maximum likelihood method: (a) Image F_1 with $\eta=10$, $\beta=45$, $\delta=6$, (b) Boundary curve F_1, (c) Image F_2 with $\eta=7$, $\beta=46$, $\delta=5$, (d) Boundary curve F_2, (e) Image F_3 with $\eta=9$, $\beta=48$, $\delta=5$ and (f) Boundary curve F_3.

The distance between $\mathcal{C}$ and ∂R can be then defined as

$$d(\partial R,\mathcal{C})=\frac{1}{N}\sqrt{\sum_{j=1}^{N}\left\|\vec{V}_j-\vec{W}_j\right\|^2}, \tag{22}$$

where N is the number of segments. This is a measure of the error committed when estimating ∂R by $\mathcal{C}$.

Algorithm 3 shows the procedure for calculating the error.

Algorithm 3 Contour Fitting Error.

```
Generate a set of test images using equation (20) and the G_A^0 distribution.
for each method do
    for each image do
        Find the fitting curve for the flower contour through the method in evaluation.
        for j = 0,...,N do
            Find the points V_j and W_j, using equation (21).
            Find the distance as in equation (22).
        end for
        Return d(∂R, C).
    end for
end for
```

With the error values calculated in Algorithm 3 for each of the test images, a graphic that serves as an aid for the comprehension of each method and that allows for comparisons between the two methods, is done.

Let e_{max} be the maximum error incured when applying this method. Let us consider the error interval

$[0, e_{max}]$ and let partition it as $\{e_0, \ldots, e_m\}$, so

$$e_i = e_0 + \Delta * i,\ i = 0, \ldots, m \tag{23}$$

where m is such that $e_{max} = e_0 + \Delta * m$ and Δ is the partition length. We define the histogram function $h : [0, e_{max}] \rightarrow \mathbf{N}$ such that

$$h(e_i) = \#\{F_k : e_i \leq d(\partial R_k, \mathcal{C}_k) < e_{i+1}\},\ i = 0, \ldots, m-1. \tag{24}$$

We call h^M the function h calculated after applying the method M. We say that a method is efficient if the values of h are high for values close to zero. We define function $h_A : [0, e_{max}] \rightarrow \mathbf{N}$, by

$$h(e_i) = \#\{F_k : d(\partial R, \mathcal{C}) \leq e_i\},\ i = 0, \ldots, m-1, \tag{25}$$

We call h_A^M the accumulated histogram function calculated for method M. A method M is more efficient than another method K if, for a given error value e_i, the condition

$$h_A^M(e_i) > h_A^K(e_i) \tag{26}$$

holds.

A Monte Carlo experience was conducted in order to assess the error committed by our proposal, using 108 simulated images according to the aforementioned model.

6 RESULTS

In this section, the error committed in the Maximum Likelihood and Anisotropic Diffusion methods, is estimated. A Monte Carlo experience was conducted in order to assess the error committed by our proposal. We generated 108 simulated images with data obeying the $\mathcal{G}_A^0(\alpha, 1, 1)$ distribution, with parameters $\alpha = -3$ for the flower and $\alpha = -10$ for the background. Then, the contour fitting error is calculated using Algorithm 3, as explained in section 5.

The result for each method is an array of values corresponding to the error committed in each test image. Then, functions $h^M(e_i)$ and $h_A^M(e_i)$, $i = 0, \ldots, m$ using equations (24) and (25), respectively, are calculated.

Figures 8 and 9 show the error histograms $h^M(e_i)$ for the methods ML and AD, respectively. In both graphics, the horizontal axis corresponds to the error intervals, and the vertical axis indicates the number of images with error within each interval.

In order to visualize the comparison between the errors for both methods, Figure 10 depicting their error histograms, is shown.

The error values shown here are between 0.0 and 1.0 because the values near zero are of more interest. It is observed that, for the ML method, most of

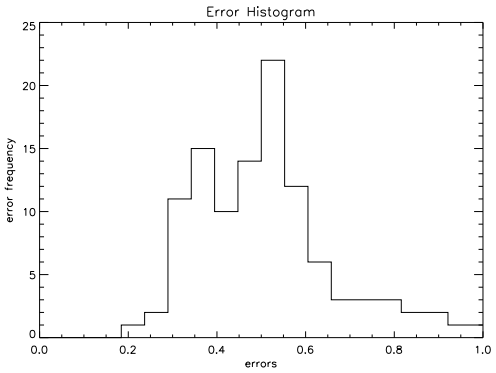

Figure 8: Error histogram for the ML method.

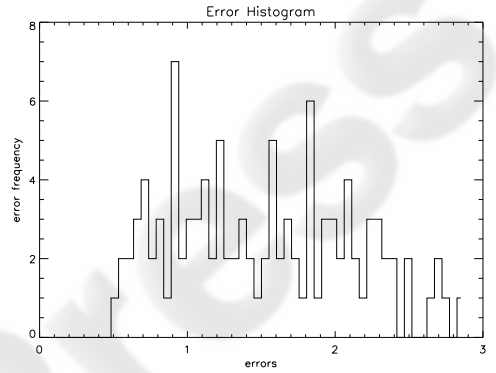

Figure 9: Error histogram for the AD method.

the images have error values less than 0.6, while for the AD method, most of the images have error values greater than 1.0. In section 7, conclusions based on these graphics are derived about the behavior of both methods.

In Figure 11 the accumulated error $h_A^M(e_i)$, given by equation 25, is shown for both methods. In this graphic it can be seen that there are 81 images with error below 1.0 for the ML method, while for the AD method there are only 26 images in that condition. It can also be seen that

$$h_A^{ML}(e) > h_A^{AD}(e) \tag{27}$$

for $e < 1.7$.

7 CONCLUSIONS

The goal of this paper was to compare two contour detection methods for speckled data: Maximum Likelihood, performed over the raw data, and Anistropic Diffusion, over estimates of the α parameter of the

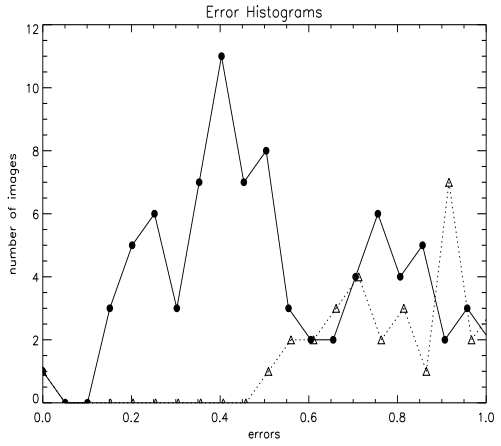

Figure 10: Error histograms for each method: the continuous line with bullets '•' corresponds to the ML method, and the dashed line with the triangles '△' corresponds to the AD method.

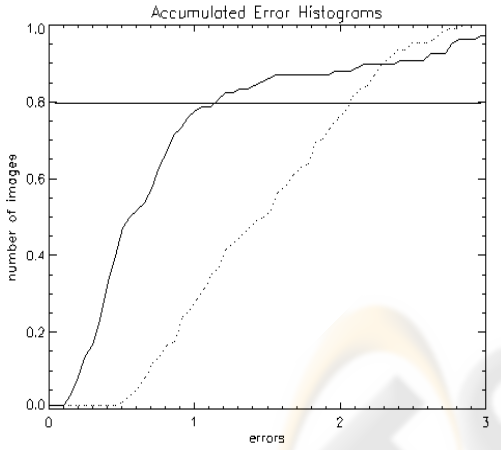

Figure 11: Accumulated errors for both methods: continuous line ML method, dashed line AD method. The horizontal line indicates 80% level.

$\mathcal{G}_A^0$ distribution. To this end, a Monte Carlo experience was conducted in which a region pattern was randomly generated and then it was submitted to both boundary fitting algorithms. The error values for the methods under study was then calculated.

In Figure 11 we observe that in the case of the Maximum Likelihood method, 80% of the segmented images have errors below 1.1, and that for the Anisotropic Diffusion method, 80% of the segmented images have errors below 1.8. This indicates that the first boundary fitting method is better than the second. Regarding the computational cost, it was also observed that Maximum Likelihood was significantly faster than Anisotropic Diffusion.

REFERENCES

Barndorff-Nielsen, O. E. and Blaesild, P. (1983). Hiperbolic Distributions. *Kotz and Johnson eds., Encyclopedia of Statistical Science, Wiley*, 3:700–707.

Blake, A. and Isard, M. (1998). *Active Contours*. Springer Verlag.

Frery, A. C., Müller, H.-J., Yanasse, C. C. F., and Sant'Anna, S. J. S. (1997). A model for extremely heterogeneous clutter. *IEEE Transactions on Geoscience and Remote Sensing*, 35(3):648–659.

Gambini, J., Mejail, M., Berlls, J. J., and Frery, A. (2006). Feature extraction in speckled imagery using dynamic b-spline deformable contours under the $\mathcal{G}^0$ models. *IJRS International Journal of Remote Sensing*. to appear.

Gambini, M. J., Mejail, M., Jacobo-Berlles, J. C., Muller, H., and Frery, A. C. (2004). Automatic contour detection in SAR images. In *Proceedings EUSAR04*.

Goodman, J. W. (1976). Some Fundamental Properties of Speckle. *Journal of the Optical Society of America*, 66:1145–1150.

Hero, A. O., Piramuthu, R., Fessler, J. A., and Titus, S. R. (1999). Minimax emission computed tomography using high-resolution anatomical side information and b-spline models. *IEEE Transactions on Information Theory*, 45(3):920–938.

Jorgensen, B. (1982). Statistical Properties of the Generalized Inverse Gaussian Distribution. *Lecture Notes in Statistic, Springer-Verlag*, 9.

Mejail, M., Jacobo-Berlles, J. C., Frery, A. C., and Bustos, O. H. (2003). Classification of SAR images using a general and tractable multiplicative model. *International Journal of Remote Sensing*, 24(18):3565–3582.

Mejail, M. E., Frery, A. C., Jacobo-Berlles, J., and Bustos, O. H. (2001). Approximation of distributions for SAR images: Proposal, evaluation and practical consequences. *Latin American Applied Research*, 31:83–92.

Perona, P. and Malik, J. (1990). Scale-space and edge detection using anisotropic diffusion. *IEEE Trans. Pattern Anal. Machine Intell.*, 12(7):629–639.

Quartulli, M. and Datcu, M. (2004). Stochastic geometrical modelling for built-up area understanding from a single SAR intensity image with meter resolution. *IEEE Transactions on Geoscience and Remote Sensing*, 42(9):1996–2003.

Rogers, D. F. and Adams, J. A. (1990). *Mathematical Elements for Computer Graphics*. McGraw-Hill, New York, USA, 2 edition.

Seshadri, V. (1993). *The Inverse Gaussian Distribution: A Case of Study in Exponential Families*. Claredon Press, Oxford, first edition.

Weickert, J. (1998). *Anisotropic Diffusion in Image Processing*. Teubner-Verlag, first edition.